Journal of Alloys and Compounds 501 (2010) 130–135

Contents lists available at ScienceDirect

Journal of Alloys and Compounds

journal homepage: www.elsevier.com/locate/jallcom

Synthesis and characterization of $Zn_{1-X}Cu_XS$ and $Zn_{1-X}Ni_XS$ nanoparticles and their applications as photocatalyst in Congo red degradation

Hamid Reza Pouretedal*, Mohammad Hossein Keshavarz

Faculty of Science, Malek-ashtsr University of Technology, Shahin-shahr, Islamic Republic of Iran

ARTICLE INFO

Article history:
Received 13 January 2010
Received in revised form 5 April 2010
Accepted 7 April 2010
Available online 18 April 2010

Keywords:
Nanocomposite
Semiconductor
Zinc sulfide
Congo red
Photocatalyst

ABSTRACT

In this work, $Zn_{1-X}Cu_XS$ and $Zn_{1-X}Ni_XS$ nanocomposites were synthesized by using a controlled co-precipitation. The nanocomposite materials were characterized by the use of UV–Vis spectra, atomic absorption spectroscopy, X-ray diffraction patterns, transmission electron microscopy image and Brunauer–Emmett–Teller method. For $Zn_{1-X}Cu_XS$ and $Zn_{1-X}Ni_XS$ nanoparticles, the X-ray diffraction patterns show the zinc-bland crystal structure. The blue shift in band-gap of ZnS was observed through incorporation of Cu^{2+} and Ni^{2+} ions. The Congo red photodegradation was performed to study the photoactivity of prepared nanocomposites under UV–Vis irradiation. The effect of dopant mole fraction, dosage of photocatalyst and pH of samples were considered on the decolorization rate of dye and photoactivity of nanocomposites. The maximum degradation of dye was obtained at pH 5–7. The $Zn_{0.94}Ni_{0.06}S$ and $Zn_{0.90}Cu_{0.10}S$ nanocomposites show the highest photoactivity. The influence of hydrogen peroxide and several anions were studied on the photoactivity of proposed catalysts. Also, the reproducibility of nanoparticles behavior as photocatalyst shows at least a four cycles of photodegradation process.

1. Introduction

A large number of studies have been devoted to the synthesis of II–VI semiconductors because of their interesting physical and chemical properties including size quantization, catalytic properties and optical properties. These semiconductors include oxides, sulfides, and selenides and so on. In particular, these semiconductors exhibit a good absorption in a visible-light region. Therefore, these compounds can be used as photocatalysts in a number of processes [1–3].

ZnS is a semiconductor with a wide band-gap semiconductor that has wide applications, e.g. UV-light emitting diodes, efficient phosphors in flat-panel displays and photovoltaic devices [4]. The doping of ZnS with transition metals such as Mn, Ni, Fe and Ag is interesting for researchers for the effect of dopant on the photoluminescence and photoactivity properties of the semiconductors. The effect of iron as dopant in the photoluminescence of ZnS nanoparticles shows a blue shift of the fundamental absorption edge by the increasing of iron. Substitution of Zn in ZnS with Fe and Ni shows similar variations in band-gap. Hence, particle size as well as the dopant concentration of X in $Zn_{1-X}M_XS$, shows a blue shift in absorption edge. While, such variations are not observed on substitution of Zn with Mn because of the sulfides of Zn and Mn are isostructural. Also, the experimental results show a considerable change in the photoluminescence spectra of ZnS nanoparticles doped with Co and Fe. Also, the lifetimes suggest a new additional decay channel of the carrier in the host material [5–7].

Textile dyes and other industrial dyestuffs constitute one of the largest groups of organic compounds, which represent an increasing environmental danger. Waste waters generated by the textile industries contain considerable amounts of non-fixed dyes, especially azo dyes, and huge amount of inorganic salts. Azo dyes with aromatic moieties linked together by azo (–N=N–) chromophores, represent the largest class of dyes used in textile processing and other industries. Approximately 50–70% of the dyes are aromatic azo compounds [8,9]. It is well known that some azo dyes and their degradation products such as aromatic amines are highly carcinogenic [10,11]. Physical methods such as adsorption, biological methods (biodegradation) and chemical methods such as chlorination and ozonation are the most frequently used methods for removal of the textile dyes from wastewater. Physical methods such as flocculation, reverse osmosis and adsorption onto activated carbon are not destructive but only transfer the contamination from one phase to another, a different kind of pollution is faced and further treatments are required. By considering these limitations, the advanced oxidation processes have been extensively investigated [12–15]. Among these processes, heterogeneous photocatalysis is found as an emerging destructive technology leading to total mineralization of most of organic pollutants.

* Corresponding author. Tel.: +98 312 591 2253; fax: +98 312 522 0420.
E-mail address: HR_POURETEDAL@mut-es.ac.ir (H.R. Pouretedal).

0925-8388/$ – see front matter © 2010 Elsevier B.V. All rights reserved.
doi:10.1016/j.jallcom.2010.04.058

The aim of this article is to study the photodegradation kinetic of Congo red (CR) catalyzed by $Zn_{1-X}Cu_XS$ and $Zn_{1-X}Ni_XS$ nanoparticles.

2. Experimental

2.1. Materials

All chemical reagents were analytical grade and prepared from Merck and Fluka Companies. Double distilled water was used to prepare aqueous solutions. The salts of $ZnCl_2$, $NiCl_2{\cdot}6H_2O$ and $CuCl_2{\cdot}2H_2O$ were used as sources of metal ions. Also, the sodium sulfide ($Na_2S{\cdot}9H_2O$) salt was used as precipitation reagent of metal ions. 2-Mercaptoethanol (2-hydroxyethanthiol, $HOCH_2CH_2SH$) was applied as capping agent in precipitation process of zinc sulfide.

The Congo red ($C_{32}H_{22}N_6Na_2O_6S_2$) stock solution with concentration of 1000 mg/L was prepared by dissolving of Congo red powder (C.I. 22120) in double distilled water. The NaOH and HCl (Merck) were used to adjust pH of samples. The salts Na_2CO_3, NaCl, Na_2SO_4 (all from Merck) were applied to study the effect of carbonate, chloride and sulfate anions on the photodegradation of dye. The isopropyl alcohol (Fluka) was used to prepare solutions of nanoparticles for UV–Vis spectra.

2.2. Preparation of nanoparticles

The nanoparticles of $Zn_{1-X}M_XS$ (M = Ni or Cu, X = 0, 0.02, 0.04, 0.06, 0.08 and 0.10) were prepared by the use of co-precipitation method in which 100 mL solution of 0.01 M Zn^{2+} and M^{2+} with mole ratio of $[M^{2+}]/[Zn^{2+}]$ = 0.00, 0.02, 0.04, 0.06, 0.08 and 0.10. Also, 50 mL solution of 0.1 M 2-mercaptoethanol was added into a three-vent balloon. Then, 100 mL solution of 0.01 M sodium sulfide ($Na_2S{\cdot}9H_2O$) was added to the balloon drop by drop by a decanter vessel under nitrogen atmosphere in which the mixture was stirred by a magnetic stirrer vigorously at the room temperature. The precipitated nanoparticles of $Zn_{1-X}M_XS$ were separated at a centrifuge with 3000–4000 rpm within 10–15 min and were washed by water and isopropyl alcohol. The cleaned particles were heated to dry in an autoclave at the temperature of 100 °C within 2 h.

2.3. Characterization of nanoparticles

The UV–Vis absorption spectra of 10 mM solutions of nanoparticles as sol transparent samples in isopropyl alcohol were recorded by a UV–Vis spectrophotometer Perkin-Elmer Lambda 2 at the room temperature. A diffractometer Bruker D8ADVANCE Germany with anode of Cu, wavelength: 1.5406 Å (Cu Kα) and filter of Ni, was used for X-ray powder diffraction (XRD) patterns. The content of M^{2+} ions (Ni^{2+} or Cu^{2+}) in $Zn_{1-X}M_XS$ was determined via atomic absorption spectrophotometer (AAS) AA-6200 Shimadzu. The size of nanoparticles was measured by a JEOL JEM-1200EXII transmission electron microscope (TEM) operating at 120 kV. The supporting grids were formvar-covered, carbon-coated, 200-mesh copper grids. BET (Brunauer–Emmett–Teller) surface area of nanoparticles was determined by Monosorb Quantochorom.

2.4. Photodegradation of Congo red

The bleaching of Congo red catalyzed by $Zn_{1-X}Ni_XS$ and $Zn_{1-X}Cu_XS$ nanoparticles was studied under UV–Vis irradiation. A photodegradation reactor system including a cylindrical Pyrex-glass cell was used to perform the experiments. A low pressure mercury vapor lamp (40 W) with radiation wavelength of 332 nm was placed in a 5 cm of Pyrex-glass cell. The photoreactor was filled with 100 mL of 5.0–20.0 mg/L of Congo red as pollutant and 0.1–1.0 g/L of nanoparticles of $Zn_{1-X}M_XS$. The temperature of the reactor was kept at 25 °C by a water-cooled jacket on its outside. A magnetic stirrer was used to ensure that the suspension of the catalyst was uniform during the course of the reaction. A Millipore membrane filters were used to collect the samples at regular intervals; and the nanoparticles were removed by centrifuge.

The absorbance of Congo red samples at λ_{max} of 510 nm was measured by an UV–Vis spectrophotometer Perkin-Elmer Lambda 2 by a paired 1.0 cm quartz cell. The decrease of absorbance of samples at λ_{max} of dye after irradiation in a certain time shows the rate of decolorization and, therefore, photodegradation efficiency of the dye. The degradation efficiency can be calculated as:

$$\%D = 100 \times \left[\frac{C_0 - C_t}{C_0}\right] = 100 \times \left[\frac{A_0 - A_t}{A_0}\right] \quad (1)$$

where C_0 and C_t are the initial concentration and the concentration of dye in time of 0 and t, respectively; A_0 and A_t are the initial absorbance and the absorbance of sample in time t, respectively; and t is the irradiation time of sample.

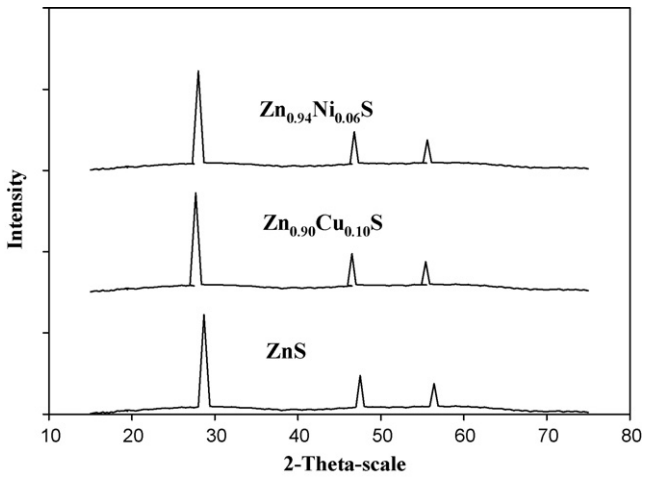

Fig. 1. X-ray diffraction patterns of ZnS, $Zn_{0.94}Ni_{0.06}S$ and $Zn_{0.90}Cu_{0.10}S$ nanocrystals.

3. Results and discussion

3.1. Characterization of nanoparticles

The X-ray diffraction of $Zn_{0.94}Ni_{0.06}S$ and $Zn_{0.90}Cu_{0.10}S$ nanosized powders at 2θ of 15–75° is indicated in Fig. 1. The nanoparticles exhibit a zinc-bland crystal structure. The three diffraction peaks at 2θ of 28.7°, 47.5° and 56.4° correspond to (1 1 1), (2 2 0) and (3 1 1) planes of the cubic crystalline ZnS [16,17]. There is a negligible shift in 2θ of peaks of $Zn_{0.94}Ni_{0.06}S$ and $Zn_{0.90}Cu_{0.10}S$ in comparison to ZnS. Apparently, this shift is due to the existence of Ni^{2+} or Cu^{2+} in crystal of ZnS. But, the XRD patterns show the absence of NiS and CuS as separately phase in the samples. The average of particles size was obtained by the Debye–Scherrer relations [18] and found to be about 2.0–10.0 nm.

The UV–Vis spectra of the solutions containing ZnS, $Zn_{0.94}Ni_{0.06}S$ and $Zn_{0.90}Cu_{0.10}S$ nanoparticles are shown in Fig. 2. The semiconductor of ZnS with band-gap of 3.68 eV shows an absorption edge in wavelength of 337 nm [19]. While, the nanoparticles of ZnS, $Zn_{0.94}Ni_{0.06}S$ and $Zn_{0.90}Cu_{0.10}S$ show absorbance edge in wavelength range of 260–280 nm. Thus, this blue shift in absorption edge is due to the decreasing of the particles size, and increasing of band-gap energy from 3.68 to 4.41–4.75 eV. Thus, increasing the band-gap energy of ZnS semiconductor is the result of decreasing particles size and doping of nickel and copper ions [6]. The transfer of electrons from valance-band to conductance-band is occurred with a suitable radiation. Therefore, electrons, e^-, and holes, h^+, are

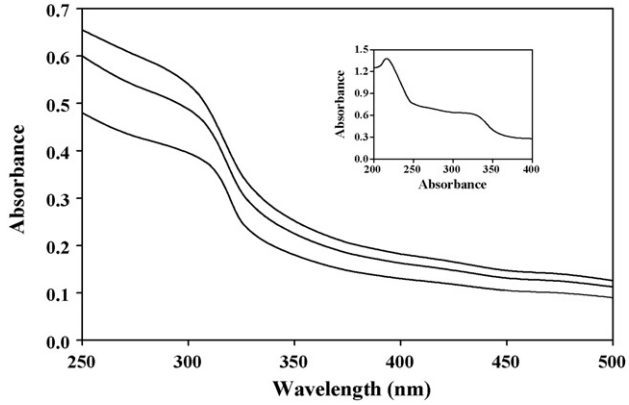

Fig. 2. UV–Vis spectra of ZnS, $Zn_{0.94}Ni_{0.06}S$ and $Zn_{0.90}Cu_{0.10}S$ nanoparticles in isopropyl solution from bottom to top. The inset of the figure shows the UV–Vis spectra of ZnS particles.

Table 1
The content of Ni^{2+} and Cu^{2+} in $Zn_{1-X}Ni_XS$ and $Zn_{1-X}Cu_XS$ nanoparticles, respectively.

The amount of X in $Zn_{1-X}M_XS$, predicted	The amount of Ni in $Zn_{1-X}Ni_XS$, determined	The amount of Cu in $Zn_{1-X}Cu_XS$, determined
0.02	0.015	0.017
0.04	0.034	0.035
0.06	0.056	0.054
0.08	0.073	0.072
0.10	0.090	0.091

formed in valance- and conductance-bands, respectively. Recombination of electrons and holes is one of the limitations of the semiconductors as photocatalyst. The increase of band-gap energy of a semiconductor determines the increasing of electrons and holes life–times. Thus, it is expected to increase the photocatalytic activity [20,21].

The content of Ni^{2+} and Cu^{2+} was determined by the use of AAS method. The amount of 0.1000 g of $Zn_{1-X}Ni_XS$ and/or $Zn_{1-X}Cu_XS$ nanoparticles dissolves in 2 M nitric acid and dilutes up to ca. 100.0 mL with double distilled water. The concentrations of Ni^{2+} and Cu^{2+} ions in sample solutions were determined from absorbance data and calibration curves. The results are summarized in Table 1. The results indicate that the doping of ZnS nanoparticles with nickel and copper ions was carried out at the desired mole fractions [22].

Fig. 3 shows the TEM image of $Zn_{0.90}Cu_{0.10}S$ nanoparticles. The nanoparticles size of <50 nm was confirmed by TEM image. Nanoparticles were probably obtained through bond of sulfur end of the 2-mercaptoethanol with sulfur in $Zn_{1-X}M_XS$ nanocomposite. 2-Mercaptoethanol covers particles of zinc sulfide and these particles do not coalesce to form bigger particles, even after an extensive period of time. Particles are suspended like colloids in solutions [23,24]. The specific surface area of nanosized particles was measured by BET method. Specific surface areas of ZnS, $Zn_{0.90}Cu_{0.10}S$ and $Zn_{0.94}Ni_{0.06}S$ were obtained 125, 132 and 128 m^2/g, respectively.

3.2. Photodegradation of Congo red

Fig. 4 shows the photodegradation efficiency of Congo red (5.0 mg/L) within 120 min at the presence of $Zn_{1-X}Ni_XS$ and $Zn_{1-X}Cu_XS$ (X = 0, 0.02, 0.04, 0.06, 0.08 and 0.10) nanoparticles with the amount of 0.1 g/L. The $Zn_{0.94}Ni_{0.06}S$ nanoparticles indicate the more photoactivity in comparison to pure ZnS nanoparticles. Also, it is indicated from Fig. 4, the highest photocatalytic efficiency was obtained in the presence of $Zn_{0.90}Cu_{0.10}S$ nanoparticles. Therefore, it is concluded that the mole fractions of 0.06 and 0.10 of Ni and Cu, respectively, are suitable to increase the reactivity of ZnS nanoparticles. For $Zn_{1-X}Cu_XS$, the doping of Cu did not show any improvement in photoactivity of catalyst in the range X > 0.10.

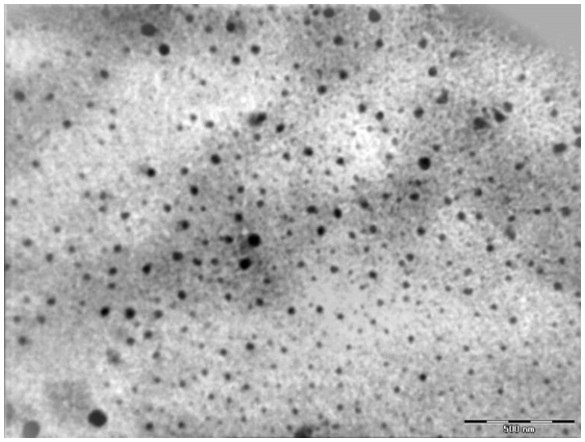

Fig. 3. TEM image of $Zn_{0.90}Cu_{0.10}S$ nanoparticles.

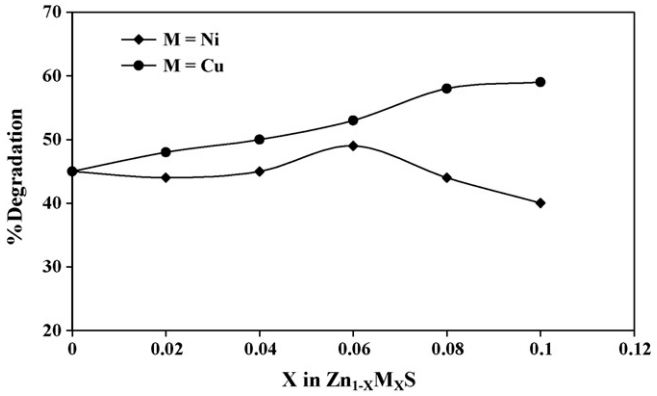

Fig. 4. The effect of mole fraction of nickel and copper dopants in $Zn_{1-X}M_XS$ nanoparticles in photodegradation of Congo red in duration time of 120 min.

The number and the lifetime of free carriers (electrons/holes) are particle size- and dopant-dependent. The high surface area to mass ratios of nanoparticles can greatly enhance the adsorption capacities of sorbent materials. There is an optimal dopant concentration that influences on the reactivity of semiconductor particles. The dopants ions serve as shallow trapping sites for the charge carriers and increase the photocatalytic efficiency by separating the arrival time of e^- and h^+ at the surface. It is possible that the dopant at high concentration acts as a trap for both e^- and h^+. Thus, the charge carriers may recombine through quantum tunneling. However, if dopant acts as an h^+ trap only, the recombination of the charge carriers is not of great concern at low dopant concentrations. Thus, an optimum dopant concentration was needed for dopant as an e^- and h^+ trap or as an h^+ trap only [25–28].

Heterogeneous photocatalysis is a complex sequence of reactions. The oxidation pathway is not yet fully understood. However, Pirkanniemi suggested in 2002 that the heterogeneous photocatalysis reaction follows five steps [28]. These are: "(i) diffusion of reactants to the surface, (ii) adsorption of reactants onto the surface, (iii) reaction on the surface, (iv) desorption of products from the surface, and (v) diffusion of products from the surface". There are two routes through which OH radicals can be formed. The reaction of the valence-band "holes" (h_{vb}^+) was occurred with either adsorbed H_2O or with the surface OH^- groups on the ZnS nanoparticle:

$$ZnS(h_{vb}^+) + H_2O_{ads} \rightarrow ZnS + {}^{\bullet}OH_{ads} + H^+ \quad (3)$$

$$ZnS(h_{vb}^+) + OH^-{}_{ads} \rightarrow ZnS + {}^{\bullet}OH_{ads} \quad (4)$$

In general, donor (D) molecules such as H_2O will be adsorbed and reacted with a hole in the valence-band. An acceptor (A) such as dioxygen will also be adsorbed and reacted with the electron in the conduction-band (e_{cb}^-). Thus, we can write:

$$ZnS(h_{vb}^+) + D_{ads} \rightarrow ZnS + D_{ads}{}^+ \quad (5)$$

$$ZnS(e_{cb}^-) + A_{ads} \rightarrow ZnS + A_{ads}{}^- \quad (6)$$

It is generally accepted that oxygen plays an important role here. Oxygen can trap conduction-band electrons to form superoxide ion ($O_2^{-\bullet}$), which can react with hydrogen ion (formed by splitting water), forming to form $HO_2^{\bullet}$:

$$ZnS(e_{CB}^-) + O_{2ads} + H^+ \rightarrow ZnS + HO_2^{\bullet} \rightarrow {}^{\bullet}O_2^- + H^+ \quad (7)$$

H_2O_2 can also be formed from $HO_2^{\bullet}$ via:

$$ZnS(e_{CB}^-) + HO_2^{\bullet} + H^+ \rightarrow H_2O_2 \quad (8)$$

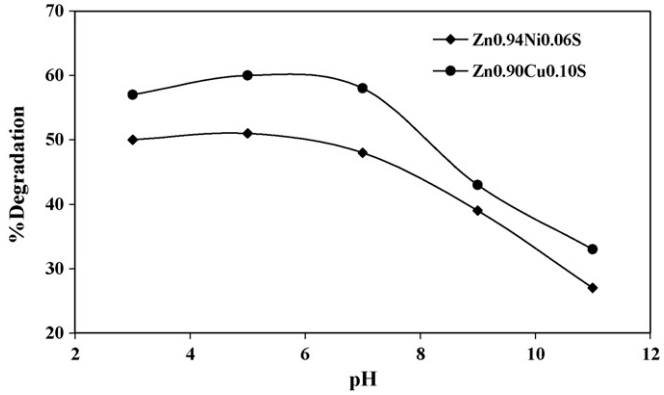

Fig. 5. The effect of pH in photodegradation of Congo red catalyzed by $Zn_{0.94}Ni_{0.06}S$ and $Zn_{0.90}Cu_{0.10}S$ nanoparticles in duration time of 120 min.

Cleavage of H_2O_2 by one of the following reactions may yield the OH radical:

$$H_2O_2 + h\nu \rightarrow 2^{\bullet}OH \quad (9)$$

$$H_2O_2 + O_2^{-\bullet} \rightarrow {}^{\bullet}OH + O_2 + OH^- \quad (10)$$

$$H_2O_2 + ZnS(e_{CB}^-) \rightarrow ZnS + {}^{\bullet}OH + OH^- \quad (11)$$

Finally, the dye degrades by the attack of direct hole and hydroxyl species [25,26]:

$$h_{vb}^+(ZnS) + \text{dye} \rightarrow \text{dye}^{\bullet+} \rightarrow \text{oxidation of the dye} \quad (12)$$

$$^{\bullet}OH_{ads} + \text{dye} \rightarrow \text{degradation of the dye} \quad (13)$$

3.3. The effect of samples pH and dosage of nanoparticles

The effect of samples pH was studied in pH range of 3–11 (Fig. 5). The pH of samples was adjusted by HCl and NaOH with concentrations of 1.0×10^{-2} M. As it is seen from Fig. 5, the highest degradation efficiency was seen in pH of 5–7 and then decreased with increasing of pH. The studies of zeta (ζ) potential show that the isoelectric point (IEP) of ZnS semiconductor is in pH of 7.0–7.5 [29]. Therefore, the surfaces of photocatalysts are positively charged in acidic solutions and negatively charged in alkaline solutions. Congo red molecule is ionized with two sulfonic groups in strong alkaline media. It becomes a soluble Congo red anion. Therefore, in the acidic and neutral solutions, Congo red molecules are easily adsorbed to the surface of ZnS nanoparticles. However, at higher pH values (pH >7), Congo red anions are generally excluded away from the negatively charged surface of ZnS nanoparticles, so, degradation yield decreases [30,31].

Fig. 6 illustrates photodegradation of Congo red in the different dosage of nanocatalysts of $Zn_{0.94}Ni_{0.06}S$ and $Zn_{0.90}Cu_{0.10}S$. After soaking in the dark within 30 min, the samples contain various amounts of nanoparticles irradiated for 120 min. The highest degradation efficiency is obtained at 0.8 g/L of nanophotocatalysts because of increasing active sites. However, the decrease of degradation at higher catalyst loading may be also due to deactivation of activated molecules by collision with ground state molecules. At the loading amount, some parts of the photocatalyst surface become unavailable for photon absorption, and dye absorption [32,33].

3.4. The effect of initial concentration of Congo red and kinetic rate constants

The photocatalytic degradation of various organic compounds such as dyes at the presence of a heterogeneous photocatalyst

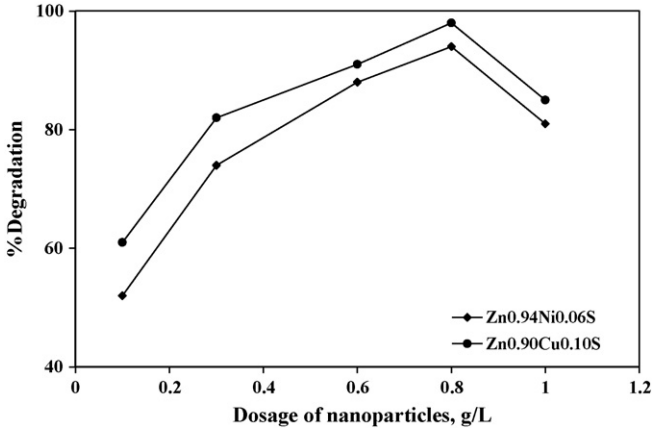

Fig. 6. The effect of dosage of $Zn_{0.94}Ni_{0.06}S$ and $Zn_{0.90}Cu_{0.10}S$ nanoparticles in photodegradation of Congo red duration time of 120 min.

can be formally described by the Langmuir–Hinshelwood kinetics model [34]:

$$r = \frac{dC}{dt} = \frac{kKC}{1 + KC} \quad (14)$$

For low concentrations of dyes ($KC \ll 1$), neglecting KC in the denominator and integrating with respect to time t, the above equation can be simplified to the pseudo-first order kinetic model equation:

$$\ln\left(\frac{C_0}{C_t}\right) = kKt = K_{app}t \quad (15)$$

where dC/dt is the rate of dye degradation (mg/L min), C_0 and C_t are initial concentration and concentration at time t of the dye (mg/L), respectively, k is reaction rate constant (min^{-1}), K is the adsorption coefficient of the dye onto the photocatalyst particle (L/mg) and k_{app} is the apparent rate constant calculated from the curves (min^{-1}). The Figs. 7 and 8 show the degradation efficiencies of Congo red in different initial concentrations versus time catalyzed by $Zn_{0.94}Ni_{0.06}S$ and $Zn_{0.90}Cu_{0.10}S$ nanoparticles, respectively. The apparent rate constants of degradation at different initial concentrations of Congo red, k_{app}, were determined from the slope of the plots of Figs. 9 and 10 in accordance to proposed kinetic model. The apparent rate constants are given in Table 2.

As seen from Table 2, the apparent rate constants of photodegradation of Congo red decrease with increasing the initial concentration of dye. More dye molecules were adsorbed on the surface of the catalyst as the initial concentration of dye increased. Thus, the generation of hydroxyl radicals at the catalyst surface

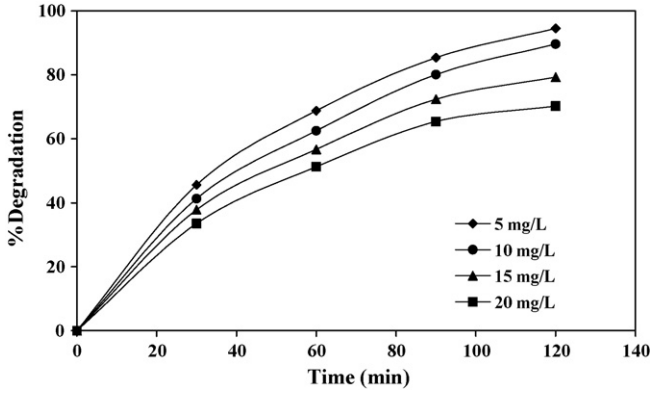

Fig. 7. The effect of initial concentration of Congo red on the degradation efficiency in the presence of $Zn_{0.94}Ni_{0.06}S$ nanoparticles(0.8 g/L) at pH 5.

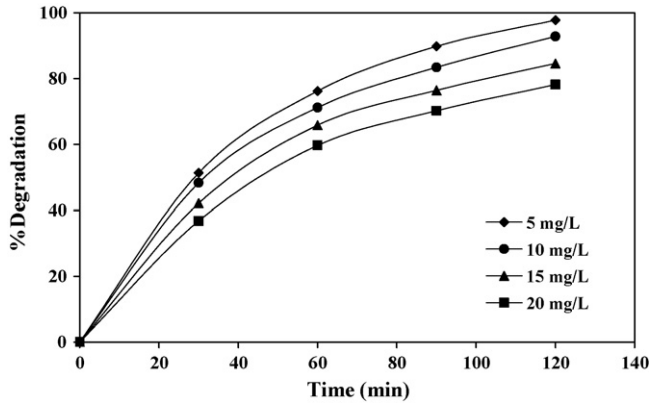

Fig. 8. The effect of initial concentration of Congo red on the degradation efficiency in the presence of $Zn_{0.90}Cu_{0.10}S$ nanoparticles (0.8 g/L) at pH 5.

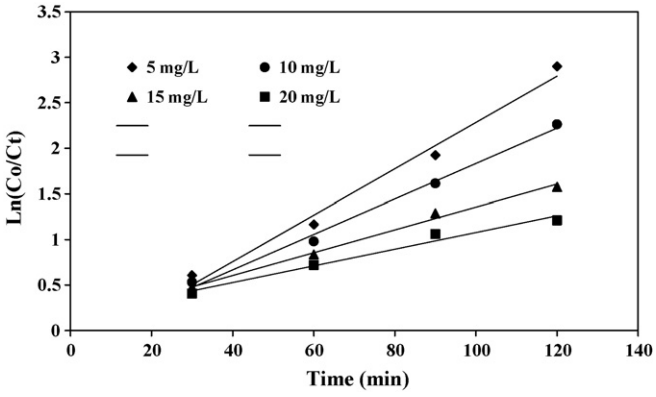

Fig. 9. Kinetic data of photodegradation of Congo red in the presence of $Zn_{0.94}Ni_{0.06}S$ nanoparticles.

Table 2
Apparent rate constants, k_{app} (min^{-1}), of Congo red degradation at different initial concentrations in the presence of $Zn_{0.94}Ni_{0.06}S$ and $Zn_{0.90}Cu_{0.10}S$ nanoparticles.

$C_{Congo\ red}$ (mg/L)	K_{app} ($Zn_{0.94}Ni_{0.06}S$)	K_{app} ($Zn_{0.90}Cu_{0.10}S$)
5.0	25.5×10^{-3}	33.8×10^{-3}
10.0	19.4×10^{-3}	21.5×10^{-3}
15.0	12.5×10^{-3}	14.5×10^{-3}
20.0	9.2×10^{-3}	11.6×10^{-3}

was reduced since the active sites were occupied by dye molecules. Moreover, as the concentration of dye increases, the dye molecules were caused to adsorb light, with the result that fewer photons could reach the photocatalyst surface [35,36].

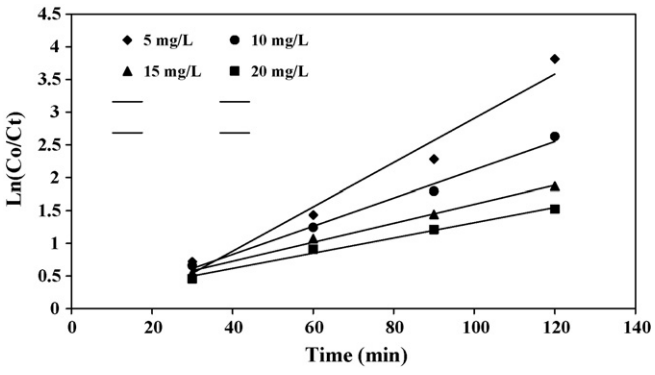

Fig. 10. Kinetic data of photodegradation of Congo red in the presence of $Zn_{0.90}Cu_{0.10}S$ nanoparticles.

3.5. Reproducibility of the photocatalysts behavior

The degradation efficiency of Congo red was shown in Fig. 11 in the presence of $Zn_{0.94}Ni_{0.06}S$ and $Zn_{0.90}Cu_{0.10}S$ nanoparticles during the four cycles of batch experiments. In each step of cycle experiments, the nanoparticles were removed, washed with water and ethanol and dried at 50 °C. The dried catalysts were used in degradation of dye under similar conditions. The decreasing of degradation yield of Congo red after four cycles was 10%.

On the other hand, the loss of Zn^{2+} ions to solutions as a result of dissolution of photocatalyst was calculated by determination of zinc ions in filtrate solutions by AAS method. Only less than 0.5% loss of zinc was seen after four cycles of reuse of $Zn_{0.94}Ni_{0.06}S$ and $Zn_{0.90}Cu_{0.10}S$ photocatalysts (0.8 g/L).

3.6. Effect of H_2O_2 concentration

The rate of Congo red (20 mg/L) photodegradation catalyzed by nanoparticles was investigated in the presence of hydrogen peroxide. The obtained results (Fig. 12) show that the rate of degradation was increased with increasing the concentration of H_2O_2 from 0 to 600 mg/L and then was decreased in higher concentrations of H_2O_2. Due to improve the rate of photocatalytic degradation of organic compounds, the oxygen and/or hydrogen peroxide can be decomposed. The mechanism of radical reactions of photodegradation can be used for explanation of this dual effect of hydrogen peroxide. In lower concentrations of H_2O_2, the added H_2O_2 accelerate the reaction through producing hydroxyl radicals from scavenging the electrons and absorption of UV-light by the following reactions:

$$H_2O_2 + e^- \rightarrow {}^\bullet OH + OH^- \quad (16)$$

$$H_2O_2 + O_2{}^{-\bullet} \rightarrow {}^\bullet OH + OH^- + O_2 \quad (17)$$

$$H_2O_2 + h\nu \rightarrow 2{}^\bullet OH \quad (18)$$

But, in higher concentrations of H_2O_2, hydrogen peroxide reacts with hydroxyal radical or acts as hole scavenger to form the perhydroxyl radicals ($HO_2{}^\bullet$), which is a much weaker oxidant than hydroxyl radicals [35,37].

$$H_2O_2 + {}^\bullet OH \rightarrow H_2O + HO_2{}^\bullet \quad (19)$$

$$H_2O_2 + h^+ \rightarrow H^+ + HO_2{}^\bullet \quad (20)$$

Thus, the photodegradation rate of Congo red reduces in higher concentrations of hydrogen peroxide (>600 mg/L) by competing H_2O_2 and dye for available hydroxyl radicals.

3.7. Effect of anions

The dye wastewater discharged from paint and dyestuff industrials often contain many organic and inorganic chemicals such as anions of salts. Thus, the photodegradation efficiency of Congo red was studied in the presence of anions such as carbonate, sulfate and chloride the same as real samples. A reduction of 3–30% in degradation efficiencies was observed with increasing the anions concentration from 250 to 1500 mg/L. The reduction of dye degradation is because of two reasons: (1) these anions can block the surface of heterogeneous catalysts and therefore, the active sites of catalysts were decreased for absorption of dye and intermediate molecules; (2) these anions could act as hydroxyl radical's scavengers [35,38]:

$$CO_3{}^{2-} + {}^\bullet OH \rightarrow CO_3{}^{-\bullet} + OH^- \quad (21)$$

$$SO_4{}^{2-} + {}^\bullet OH \rightarrow SO_4{}^{-\bullet} + OH^- \quad (22)$$

$$Cl^- + {}^\bullet OH \rightarrow Cl^\bullet + OH^- \quad (23)$$

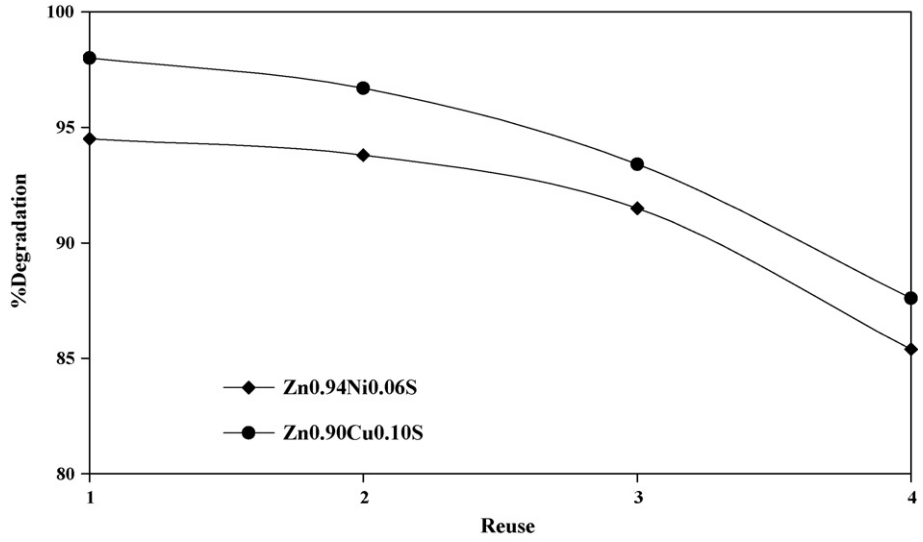

Fig. 11. Reproducibility behavior of $Zn_{0.94}Ni_{0.06}S$ and $Zn_{0.90}Cu_{0.10}S$ nanoparticles as photocatalyst in photodegradation of Congo red.

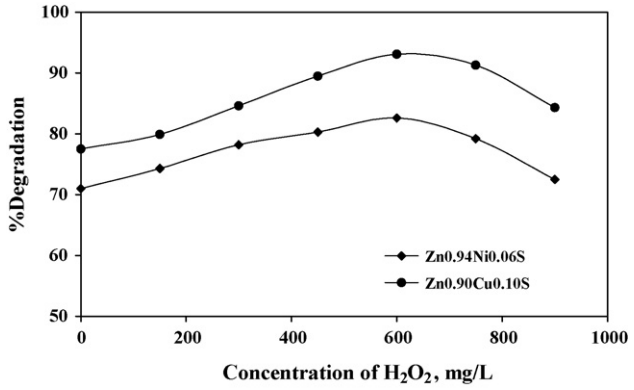

Fig. 12. The effect of H_2O_2 concentration on the photodegradation of Congo red (20 mg/L) catalyzed by $Zn_{0.94}Ni_{0.06}S$ and $Zn_{0.90}Cu_{0.10}S$ nanoparticles (0.80 g/L) at pH 5 in duration time 120 min.

The products of reactions of Eqs. (21)–(23) are radicals and hydroxide ions. But, oxidation potential of radicals is less positive than hydroxyl radicals [38]. Thus, the reducing of •OH concentration determines the decreasing of photodegradation efficiency.

4. Conclusions

A simple controlled-precipitation method can be applied to prepare $Zn_{1-X}M_XS$ nanoparticles with Ni and/or Cu dopants. The prepared nanoparticles show a catalytic activity in Congo red photodegradation process. The mole fractions of 0.06 and 0.10 for nickel and copper, respectively, in $Zn_{1-X}M_XS$ nanoparticles show the highest photocatalytic activity at pH 5 and 0.80 g/L of catalyst within 120 min. The kinetic rate constants of degradation were decreased by the increasing of initial concentration of Congo red. The degradation efficiencies decrease in the presence of anions that are usually in real water samples. An increase of degradation efficiency up to 20% was observed in the presence of 600 mg/L hydrogen peroxide as an oxidant.

References

[1] J.Y. Shi, H.J. Yan, X.L. Wang, et al., Solid State Commun. 146 (2008) 249–252.
[2] L.Z. Wang, Y. Jiang, C. Wang, et al., J. Alloys Compd. 454 (2008) 255–260.
[3] S.H. Shen, L. Zhao, L.J. Guo, Mater. Res. Bull. 44 (2009) 100–105.
[4] K. Jayanthi, S. Chawla, H. Chander, D. Haranath, Cryst. Res. Technol. 42 (2007) 976–982.
[5] S. Sambasivam, B.K. Reddy, A. Divya, N. Madhusudhana Rao, C.K. Jayasankar, B. Sreedhar, Phys. Lett. A 373 (2009) 1465–1468.
[6] H.R. Pouretedal, A. Norozi, M.H. Keshavarz, A. Semnani, J. Hazard. Mater. 162 (2009) 674–681.
[7] S.L. Shah, W. Li, C.P. Huang, O. Jung, C. Ni, Colloquium 99 (2002) 6482–6486.
[8] R. Molinari, F. Pirillo, M. Falco, V. Loddo, L. Palmisano, Chem. Eng. Process 43 (2004) 1103–1114.
[9] S. Bilgi, C. Demir, Dyes Pigments 66 (2005) 69–76.
[10] K.I. Konstantinou, A.A. Triantafyllos, Appl. Catal. B: Environ. 49 (2004) 1–14.
[11] Z. Zhang, Y. Shan, J. Wag, H. Ling, S. Zang, W. Gao, Z. Zhao, H. Zhang, J. Hazard. Mater. 147 (2007) 325–333.
[12] C. Guillard, H. Lachheb, A. Houas, M. Ksibi, E. Elaloui, J.M. Herrmann, J. Photochem. Photobiol. A: Chem. 158 (2003) 27–36.
[13] C. Hachem, F. Bocquillon, O. Zahraa, M. Bouchy, Dyes Pigments 49 (2001) 117–125.
[14] V. Augugliaro, C. Baiocchi, A.B. Prevot, E.G. Lopez, V. Loddo, S. Malato, G. Marci, L. Palmisano, M. Pazzi, E. Pramauro, Chemosphere 49 (2002) 1223–1230.
[15] I.A. Alaton, I.A. Balcıŏglu, D.W. Bahnemann, Water Res. 36 (2002) 1143–1154.
[16] V.T. Liveri, M. Rossi, G. D'Arrigo, D. Manno, G. Micocci, Appl. Phys. A 69 (1999) 369–373.
[17] H.C. Warad, S.C. Ghosh, B. Hemtanon, C. Thanachayanont, J. Dutta, Sci. Technol. Adv. Mater. 6 (2005) 296–301.
[18] A. Guinier, X-ray Diffraction, San Francisco, CA, 1963.
[19] P. Yang, M. Lu, D. Xu, D. Yang, J. Chang, G. Zhou, M. Pan, Appl. Phys. A 74 (2002) 257–259.
[20] M. Qamar, M. Saquib, M. Muneer, Desalination 186 (2005) 255–271.
[21] M.R. Hoffmann, S.T. Martin, W. Choi, D.W. Bahnemann, Chem. Rev. 95 (1995) 69–85.
[22] P.V.B. Lakshmi, K.S. Raj, K. Ramachandran, Cryst. Res. Technol. 44 (2009) 153–158.
[23] H.Z. Zeng, K.Q. Qiu, Y.Y. Du, W.Z. Li, Chin. Chem. Lett. 18 (2007) 483–486.
[24] P.H. Borse, N. Deshmukh, R.F. Shinde, S.K. Date, S.K. Kulkarni, J. Mate. Sci. 34 (1999) 6087–6093.
[25] D. Beydoun, R. Amal, G. Low, S. McEvoy, J. Nanoparticle Res. 1 (1999) 439–458.
[26] C. Hu, Y.Z. Wang, Chemosphere 39 (1999) 2107–2115.
[27] K. Dhermendra, J. Tiwari, J. Behari, P. Sen, World Appl. Sci. J. 3 (2008) 417–433.
[28] K. Pirkanniemi, M. Sillanpaa, Chemosphere 48 (2002) 1047–1060.
[29] M.S. Moignard, R.O. James, T.W. Healy, Aust. J. Chem. 30 (1977) 733–740.
[30] S. Erdemŏglu, S. Aksub, F. Sayılkan, B. Izgi, M. Asiltürk, H. Sayılkan, F. Frimmel, S. Güçer, J. Hazard. Mater. 155 (2008) 469–476.
[31] K. Melghit, S.S. Al-Rabaniah, J. Photochem. Photobiol. A: Chem. 184 (2006) 331–334.
[32] H.R. Pouretedal, H. Eskandari, M.H. Keshavarz, A. Semnani, Acta Chim. Slov. 56 (2009) 353–361.
[33] B. Gözmena, M. Turabik, A. Hesenov, J. Hazard. Mater. 164 (2009) 1487–1495.
[34] H. Al-Ekabi, N. Serpone, J. Phys. Chem. 92 (1988) 5726–5731.
[35] M.A. Behnajady, N. Modirshahla, R. Hamzavi, J. Hazard. Mater. 133 (2006) 226–232.
[36] R.W. Matthews, J. Phys. Chem. 91 (1987) 3328–3333.
[37] H. Zhao, S. Xu, J. Zhong, X. Bao, Catal. Today 93–95 (2004) 857–861.
[38] M. Bekbolet, I. Balcioglu, Water Sci. Technol. 34 (1996) 73–80.